Title

IL-7 production in murine lymphatic endothelial cells and induction in the setting of peripheral lymphopenia

Journal

International Immunology, 25(8)

ISSN

0953-8178

Authors

Miller, Corey N

Hartigan-O'Connor, Dennis J

Lee, Myeong Sup

et al.

Publication Date

2013-08-01

DOI

10.1093/intimm/dxt012

Peer reviewed

International Immunology, Vol. 25, No. 8, pp. 471–483
doi:10.1093/intimm/dxt012
Advance Access publication 8 May 2013

FEATURED ARTICLE

IL-7 production in murine lymphatic endothelial cells and induction in the setting of peripheral lymphopenia

Corey N. Miller[1,*], Dennis J. Hartigan-O'Connor[1,2,*], Myeong Sup Lee[3,*], Grace Laidlaw[4], Ivo P. Cornelissen[5,7], Mehrdad Matloubian[6], Shaun R. Coughlin[5], Donald M. McDonald[4] and Joseph M. McCune[1]

[1]Division of Experimental Medicine, Department of Medicine, University of California, San Francisco, CA 94110, USA
[2]Department of Medical Microbiology and Immunology and California National Primate Research Center, University of California, Davis, CA 95616, USA
[3]Department of Biochemistry and Genome Research Center, Yonsei University, South Korea
[4]Department of Anatomy and Helen Diller Cancer Center, University of California, San Francisco, CA 94143, USA
[5]Cardiovascular Research Institute, University of California, San Francisco, CA 94158, USA
[6]Division of Rheumatology, Department of Medicine, University of California, San Francisco, CA 94143, USA
[7]Present address: Vesalius Research Center, Leuven, Belgium

Correspondence to: J. M. McCune, Division of Experimental Medicine, University of California, San Francisco, UCSF Box 1234, CA 94143-1234, USA; E-mail: mike.mccune@ucsf.edu

* These individuals are co-first authors and are listed in order of the relative importance of their substantial contributions to this study.

Received 4 September 2012, *accepted* 5 March 2013

Abstract

IL-7 is a required factor for T-cell homeostasis. Because of low expression levels and poor reagent availability, the cellular sources of IL-7 have proven challenging to characterize. In this study, we describe a reporter mouse in which enhanced GFP is expressed from the endogenous *Il7* locus. We show that IL-7 is produced by lymphatic endothelial cells (LECs) distributed throughout the systemic lymphatic vasculature as well as by fibroblastic reticular cells, and that phosphorylation of STAT5 in lymphocytes is higher in lymphatics than in blood. Furthermore, in nodes depleted of lymphocytes, *Il7* transcription is increased in stromal but not in myeloid subsets. These data support recent findings that lymphocyte homeostasis is influenced by access to secondary lymphoid organs and point to LECs as an important *in vivo* source of IL-7, bathing trafficking immune cells under both resting and lymphopenic conditions.

Keywords: endothelium, HIV, interleukin-7, lymphatic, lymph node, lymphopenia, myeloid, stromal

Introduction

IL-7 is a member of the type I cytokine family and a non-redundant regulator of T-cell development and peripheral T-cell homeostasis (1, 2). The absolute requirement for IL-7 signaling during lymphocyte development in the bone marrow (BM) and thymus is underscored by the paucity of T, B and thymic NK cells in *Il7*- and *Il7r*-deficient mice as well as by the absence of T cells in human patients harboring a dysfunctional IL-7R or common γ chain (3–5).

We previously reported that circulating levels of IL-7 are inversely correlated with $CD4^+$ T-cell counts in the context of HIV-associated lymphopenia (6). This effect was most dramatic in patients with T-cell counts below 200 cells/μl, in whom plasma IL-7 levels were elevated by up to 10-fold. To better understand the possible sources of IL-7 in these patients, immunohistochemistry was performed on lymphocyte-replete or lymphocyte-depleted lymph node (LN) samples from individual patients in this study. Both the frequency and intensity of IL-7 protein staining were increased within a small subset of LN-resident cells in the most lymphocyte-depleted tissues. Interestingly, co-staining analysis revealed that some of the IL-7-producing cells were positive for phenotypic markers suggestive of myeloid lineage (e.g. S100b and CD68) (6).

Multiple reports have now established an inverse correlation between the number of circulating peripheral T cells and blood IL-7 levels in humans (7, 8). In the context of HIV infection and progression to AIDS, this relationship could be

the result of several possible mechanisms: sensor cells may exist in the periphery that respond to the size of the peripheral T-cell compartment by adjusting their expression of IL-7 in a homeostatic feedback loop; factors associated with HIV infection and/or with the subsequent immune response against HIV might alter IL-7 expression and/or T-cell depletion in the periphery may passively permit IL-7 accumulation.

It is thought that IL-7 is produced primarily by adherent stromal cells in tissues throughout the body. BM reticular cells are a major source of IL-7 (9, 10) as may be osteoblasts (11). In the thymus, reticular epithelial cells of the sinus and corticomedullary junction have been shown by *in situ* hybridization and *in vitro* analysis to be an important IL-7-producing subset, whereas thymic dendritic cells (DCs) have also been implicated (12–14). Cells producing IL-7 have been found within the spleen, LN, liver, lung, skin and intestine (15–20). Although specific adherent cell types such as the fibroblastic reticular cells (FRCs) of LNs have been identified as IL-7 source cells (16), many cellular sources remain incompletely characterized. Most recently, IL-7 production by the FRC subset was confirmed by two independent groups and lymphatic endothelial cells (LECs) were suggested to be another source of IL-7 (21, 22).

Some studies suggest that *Il7* expression is constitutive and not subject to active regulation (23), whereas other studies have found that *Il7* expression is regulated by immune modulators such as TGF-β, TNF-α and interferon (24–27) and, for example, may be up-regulated by epithelial cells at surface barriers upon microbial exposure (27). In this vein, it was recently shown that the liver might be an important source of the cytokine during systemic immune activation, where *Il7* was induced by inflammatory stimuli such as lipopolysaccharide and CpG (19).

In this study, we hypothesized that IL-7 production in the periphery is triggered in cells that can 'sense' lymphopenia and/or pathogen challenge. To facilitate characterization of such putative IL-7-producing cells, we generated a reporter mouse in which enhanced GFP (eGFP) is expressed under control of the endogenous *Il7* promoter.

Methods

Mice

Il7-eGFP knock-in mice were generated using a standard embryonic stem (ES) cell gene-targeting strategy (Fig. 1A). The details of the mouse generation, Southern blot analysis and routine screening by PCR are provided in the Supplementary Appendix, available at *International Immunology* Online. Homozygous *Il7*$^{eGFP/eGFP}$ mice derived by crossing heterozygous *Il7*$^{+/eGFP}$ mice were born at the expected Mendelian ratios, fertile and healthy.

For BM transplantation experiments, B6 CD45.1 mice were obtained from The Jackson Laboratory (Bar Harbor, ME, USA). Details of the preparation of BM chimeras are provided in the Supplementary Appendix, available at *International Immunology* Online. Mice were housed under specific pathogen-free conditions. All experimental procedures were approved by the institutional animal care and use committee of the University of California, San Francisco.

Sampling and counting of blood and LN cells

Whole blood (10 μl) was collected from the saphenous vein, anti-coagulated with 10 mM EDTA in PBS, stained for flow analysis, lysed to remove RBCs and fixed. Individual inguinal LNs or pooled LNs (inguinal, axillary, brachial and mesenteric) were processed as described (see 'Preparation of single-cell suspensions from tissues') to obtain single-cell suspensions. The resultant cells were stained for flow analysis and fixed (see 'Flow cytometric analysis and cell sorting'). Samples were stained with a cocktail of antibodies directed against CD3, CD4 and CD8 or CD3 and B220, analyzed and counted using a C6 Cytometer (BD Biosciences, San Jose, CA, USA).

Preparation of single-cell suspensions from tissues

LNs (inguinal, axillary, brachial and mesenteric) and lungs were harvested, pooled and coarsely minced from five mice. Tissues were digested with rotation at 37°C in 5 ml of digestion medium containing a 1:300 dilution of Blendzyme (Roche, Indianapolis, IN, USA) and 20 μg/ml DNase I in RPMI 1640. Tissue fragments were triturated every 30 min through a wide-bore pipette tip and the digestion medium was replaced after 1 h. This process was repeated twice or until no visible fragments remained. The single-cell suspension was mixed 1:1 with digestion stop solution containing 10% fetal bovine serum and 10 mM EDTA in RPMI 1640, and kept on ice until further processing. Cells were separated from tissue debris by straining through a 45-μm mesh and washed twice in FACS buffer (containing 2% fetal bovine serum and 2 mM EDTA in PBS) in preparation for antibody staining.

Collection of cells from efferent lymphatics

Lymph was drawn from the large lymphatic vessel adjacent to the superior mesenteric artery of mice anesthetized with a cocktail of ketamine (100 mg/kg) and xylazine (10 mg/kg). The vessel was exposed under a dissecting microscope and cannulated with a hand-drawn glass needle. Fluid was drawn via mouth pipette until 20–50 μl had been collected.

Flow cytometric analysis and cell sorting

Cells were stained at a maximum density of 20×10^6 cells/ml in FACS buffer. For some experiments, CD45$^+$ hematopoietic cells were removed by immunomagnetic bead depletion (Miltenyi, Auburn, CA, USA) before staining. All staining was performed for 30 min at 4°C and all washes were done twice at room temperature in FACS buffer. Antibodies for staining were from Biolegend (San Diego, CA, USA; B220-A700, CD3-PE, CD43-APC, CD45-A700, CD45.1-A700, CD45.2-PE, EpCAM-PE-Cy7, gp38-PE, gp38-APC and HSA-PB), eBioscience (San Diego, CA, USA; BP1-PE, CD4-APC, CD8-PerCP-Cy5.5, CD11b-PB and CD11c-A700), BD Biosciences (I-A/I-E-PE, pSTAT5-PE and pSTAT5-A647) and Invitrogen (Carlsbad, CA, USA; CD31-PB). Events were collected on a BD LSRII or ARIA2. For cell sorting and RT–PCR analysis, $5–20 \times 10^3$ events were sorted directly into 500 μl of TRIzol reagent and the resultant lysates were frozen at −80°C until further processing. Phosflow analysis for detecting intracellular pSTAT5 was performed using BD LyseFix and Perm Buffer III (BD Biosciences), according to the manufacturer's instructions.

Quantitative RT–PCR

RNA was extracted by phenol–chloroform extraction or with the Omniscript (Qiagen, Germantown, MD, USA) kit. cDNA was generated using the VILO kit (Invitrogen) and samples were

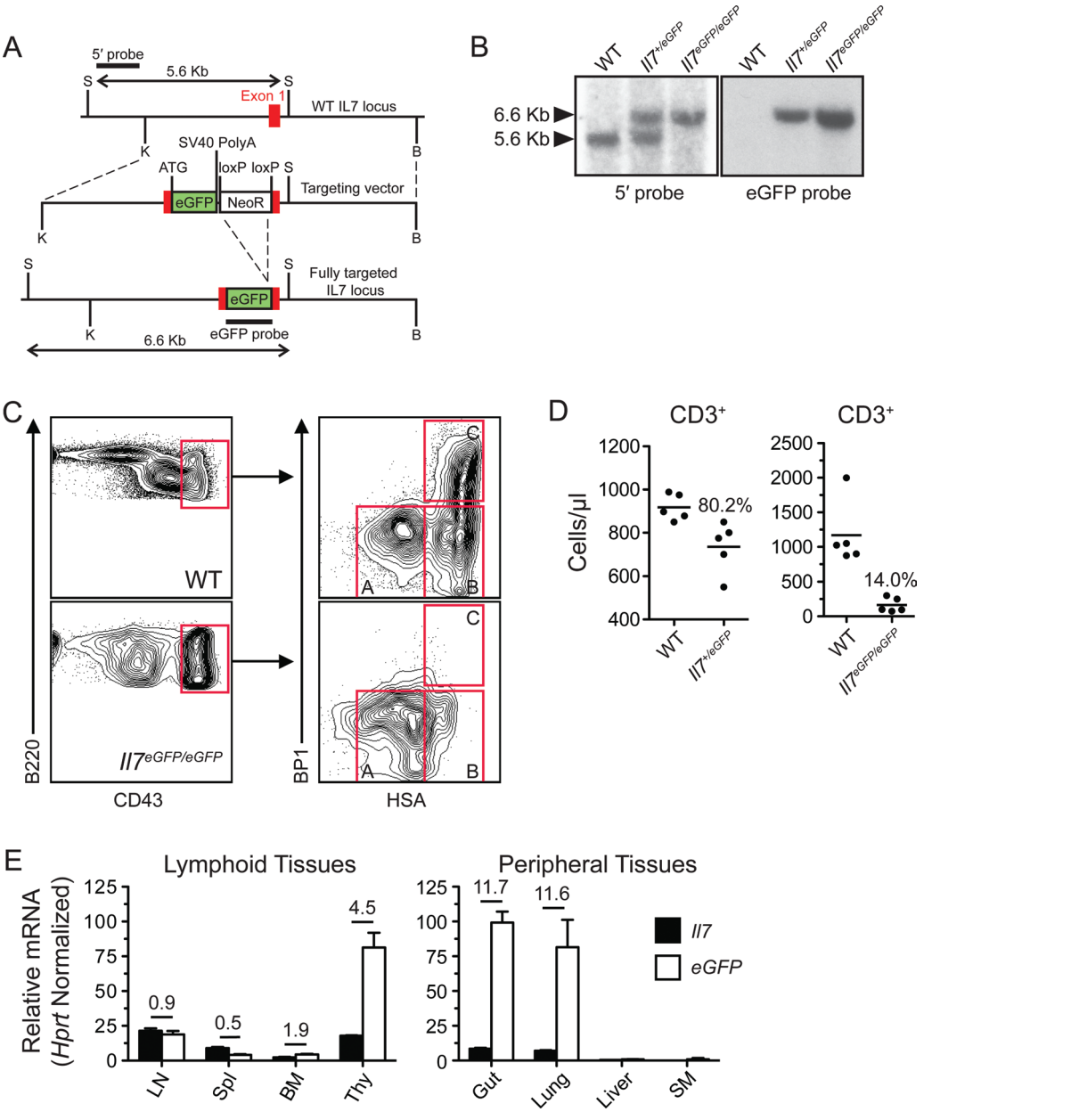

Fig. 1. *Il7-eGFP* reporter mice are correctly targeted and report *Il7* transcription with fidelity. (A) Knock-in targeting strategy for generating *Il7-eGFP* reporter mice. S, *SacI*; K, *KpnI*; B, *BamHI*. eGFP, *eGFP* coding sequence; *NeoR*, neomycin-resistance gene cassette. (B) Southern blot analysis of tail genomic DNA digested with the restriction endonuclease *SacI*. The WT allele is expected to yield a 5.6-kb fragment, whereas the final targeted, *NeoR*-deleted allele is expected to yield a 6.6-kb fragment. (C) Flow cytometry analysis of single-cell suspensions prepared from WT or *Il7*$^{eGFP/eGFP}$ BM and stained with antibodies against B220, CD43, HSA and BP1. Fractions A–C, Hardy B-cell developmental fractions: pre-pro B cells (Hardy A) and pro B cells (Hardy B). (D) Absolute lymphocyte counts in whole blood collected from WT, *Il7*$^{+/eGFP}$ or *Il7*$^{eGFP/eGFP}$ mice stained with antibodies against CD3, CD4 and CD8. Percentage is compared with WT. (E) Quantitative RT–PCR analysis of whole-tissue RNA collected from lymphoid (LN, inguinal LNs Spl, spleen; BM, bone marrow; Thy, thymus) or non-lymphoid tissues (gut; lung; liver; SM, skeletal muscle). Ratio of *eGFP* signal to *Il7* signal (*eGFP:Il7*) is indicated. Data are representative of at least two independent experiments with at least five mice per group.

amplified using Taqman 2× PCR Mastermix and the Step One Plus System (Applied Biosystems, Carlsbad, CA, USA). Further details and primer/probes are provided in the Supplementary Appendix, available at *International Immunology* Online.

Immunofluorescent analysis of tissue

Mice were perfused with 1% paraformaldehyde for 2 min and tissues were harvested and drop-fixed at room temperature for an additional 1 h. An antibody cocktail prepared by re-suspending 100 µg of rabbit monoclonal anti-GFP antibody (GFP ABfinity; Invitrogen) in 200 µl rabbit polyclonal anti-GFP antibody (A-11122; Invitrogen) was used for eGFP staining. For whole-mount immunostaining of diaphragms, eGFP antibody cocktail (1:750) and rat monoclonal antibody (ALY7, 1:500; eBioscience) against LYVE1 were used. Tissues were cleaned of excessive fat and muscle surrounding the central

tendon, and stained overnight with the primary antibodies at room temperature followed by washing in 0.3% Triton/PBS for 8 h, as previously described (28). Goat secondary antibodies labeled with FITC or Cy3 were used at 1:500 (Jackson ImmunoResearch Laboratories, West Grove, PA, USA) and incubated overnight at room temperature. Tissues were washed for 2 h and mounted in Vectashield with 4',6-diamidino-2-phenylindole. For tissue sections, LNs and lung were cryoprotected in 30% sucrose/PBS overnight and embedded in Tissue-Tek OCT (Sakura Finetek, Torrance, CA, USA). About 20- (LNs) or 200-μm (lung) sections were cut and stained on slides or floated in six-well dishes, respectively. LN sections were stained for eGFP with the rabbit antibody cocktail described in "Flow cytometric analysis and cell sorting" (1:1250), for LYVE1 with rat monoclonal antibody (ALY7, 1:500; eBioscience) and for CD11b with rat monoclonal antibody (M1/70.15, 1:500; AbD Serotec). The eGFP signal was amplified using Tyramide Signal Amplification (Alexa 488; Invitrogen) followed by co-staining for other markers with goat secondary antibodies, as directed by the manufacturer. Thick lung sections were stained as for the diaphragm whole mounts. Images were acquired with a Zeiss Axiophot confocal microscope.

Blockade of lymphocyte ingress into the LNs

Mice were injected intra-peritoneally with 100 μg of anti-α_4 integrin antibody (clone M17/4) and 100 μg of anti-α_L integrin antibody (clone PS/2) in PBS every other day to maintain blockade of lymphocyte ingress into the LNs for up to 22 days. Lymphocyte depletion was monitored by FACS analysis.

Statistical analysis

Statistical analysis was performed using GraphPad Prism software (GraphPad Software, Inc., La Jolla, CA, USA). Statistical significance was determined with an unpaired two-tailed Student's *t*-test and details of the tests employed are given in figure legends alongside the corresponding *P* values.

Results

Il7-eGFP reporter mouse construction

To generate a reporter that accurately reflects *Il7* expression under physiologic conditions, the *eGFP* gene was introduced directly into the endogenous *Il7* locus using a standard ES cell gene-targeting strategy. The gene-targeting vector developed for this purpose replaces most (191-bp region upstream of the start codon) of the 247-bp *Il7* 5′ untranslated region (UTR) and inserts the *eGFP* coding sequence followed by an *SV40 polyA* signal sequence at the start codon of the *Il7* gene (Fig. 1A and 'Methods'). Insertion of *eGFP* at the start codon is expected to prevent *Il7* expression from the targeted allele. Heterozygous *Il7-eGFP* knock-in ($Il7^{+/eGFP}$) mice were derived from chimeric founders using a standard breeding strategy. Correct targeting and insertion of a single copy of *eGFP* were verified by Southern hybridization of restriction endonuclease-digested genomic tail DNA with an external 5′ probe and internal eGFP probe, respectively (Fig. 1B; data not shown)

To confirm that *eGFP* targeting resulted in a functional knockout (KO) of *Il7*, we compared the phenotype of $Il7^{eGFP/eGFP}$ homozygotes to that of the well-characterized $Il7^{-/-}$ and $Il7r^{-/-}$ mice (3, 5). FACS analysis of dispersed $Il7^{eGFP/eGFP}$ BM cells revealed that B-cell development was arrested at the pre-pro B-cell developmental stage (Fig. 1C) and thymic tissue was hypoplastic, with a severe reduction in the number of mature single-positive thymocytes (data not shown). In the periphery, LNs were absent or small, with the exception of mesenteric nodes, which were reduced in frequency but of normal macroscopic appearance and size. Although the spleens of $Il7^{eGFP/eGFP}$ mice were normal in size and appearance, the peripheral $CD3^+$ T-lymphocyte count was 14% of the normal value observed in wild-type (WT) littermates (Fig. 1D). These results closely matched with those reported for $Il7^{-/-}$ and $Il7r^{-/-}$ mice, indicating that $Il7^{eGFP/eGFP}$ mice are indeed deficient in IL-7 (3, 5).

Il7-eGFP heterozygotes report Il7 transcription with fidelity

Although $Il7^{eGFP/eGFP}$ mice display the severe congenital defects associated with a complete lack of IL-7, only a mild defect in lymphocyte homeostasis would be expected in *Il7-eGFP* heterozygotes. Compared with WT littermate controls, the spleen and thymus of *Il7-eGFP* heterozygotes appeared normal, LNs were slightly reduced in size and peripheral $CD3^+$ T-lymphocyte counts were modestly reduced (by 10–20%) (Fig. 1D and data not shown). Given such a robust peripheral lymphocyte compartment, we considered that the *Il7-eGFP* reporter model would be useful for interrogating the effects of experimentally induced lymphocyte depletion on *Il7* expression.

To test whether the expression of *eGFP* transcript reflected that of *Il7* transcript, whole-tissue RT–PCR analysis was performed on a range of tissues. All tissues expressing *Il7* were also found to express *eGFP*, whereas those with low or undetectable *Il7* expression had low or undetectable *eGFP* expression (Fig. 1E). LNs, spleen and BM showed excellent agreement (within a 2-fold range) between expression of *Il7* and that of the reporter, whereas thymus, gut and lung showed considerably more (>4-fold) *eGFP* than *Il7* expression (Fig. 1E). This overall pattern not only confirmed that *Il7*-expressing tissues reliably expressed *eGFP* but also suggested that IL-7 protein expression is limited in some specific cell types by endogenous control elements missing from the *eGFP* transcript. Thus, in subsequent experiments, detection of eGFP protein was used to assist in identification of IL-7-producing cell types, but endogenous *Il7* transcripts were also assessed to assure correct identification of those cells and quantification of *Il7* transcript levels.

FRCs and LECs are the dominant source of IL-7 within resting LNs

Initial immunofluorescence evaluation of the *Il7-eGFP* reporter revealed significant eGFP signal within both the cortex and medulla of the thymus that was localized to large reticular epithelial complexes, in agreement with recent reports (Supplementary Figure 1A, available at *International*

Immunology Online) (21, 22). To determine the distribution of reporter protein within resting LNs, inguinal LN sections from *Il7*$^{+/eGFP}$ mice were immunostained for eGFP. Unexpectedly, signal was restricted to the subcapsular sinus and extended into the medullary region, with occasional projections around B-cell follicles (Fig. 2A and B). The predominant cell types with this distribution pattern are thought to be LECs lining the sinus and closely associated subcapsular and medullary

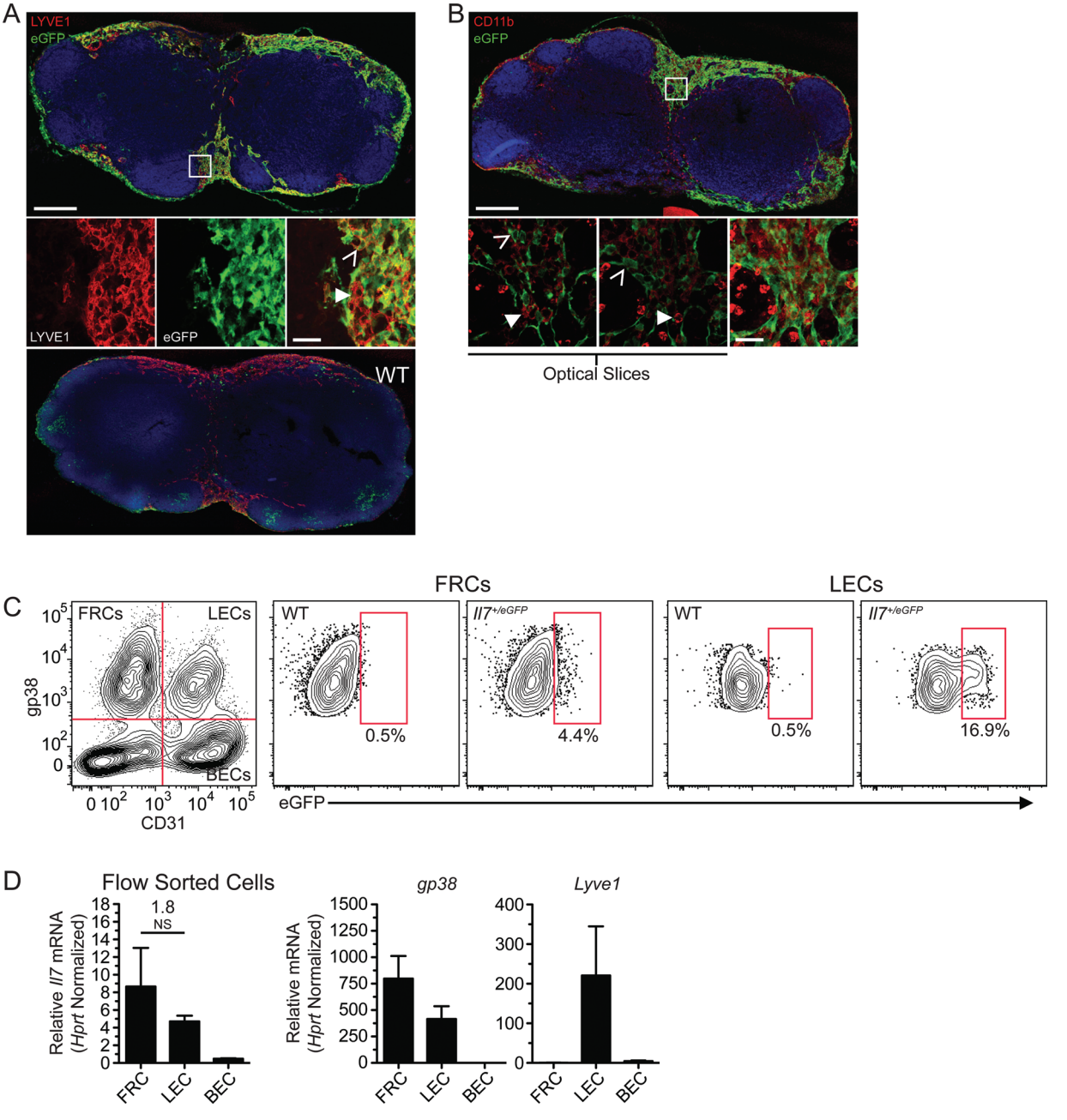

Fig. 2. LECs are an important source of IL-7 within the resting LN. (A and B) Confocal immunofluorescence microscopy of perfusion-fixed inguinal LNs from *Il7*$^{+/eGFP}$ or WT control mice. Data are representative of two separate experiments with three mice per group. Low-magnification scale bars represent 200 μm and high-magnification scale bars represent 20 μm. (A) eGFP (green) is localized to the subcapsular sinus and medullary region and co-localizes with LYVE1 (red). Open arrow in high-magnification overlay points to eGFP^{+}LYVE1^{+} double-positive LEC and closed arrow points to eGFP^{-} LEC. eGFP staining in WT node is shown in the bottom panel. (B) Subcapsular and medullary eGFP (green) does not co-localize with the myeloid marker CD11b (red) in optical slices from the confocal stack. Open arrows point to eGFP^{+} cells that are non-overlapping with CD11b^{+} cells (closed arrows). (C and D) Analysis of pooled single-cell suspensions prepared by enzymatic digestion of LNs from *Il7-eGFP* heterozygote or WT littermate control mice. Stromal subsets enriched by CD45^{+} cell depletion were stained for CD45, gp38 and CD31. (C) eGFP signal is localized to the FRC and LEC subsets. (D) Quantitative RT–PCR analysis of *Il7*, *gp38* and *LYVE1* transcripts on flow-sorted FRCs, LECs and BECs from WT mice. Fold difference in *Il7* levels between FRCs (CD31^{-}gp38^{+}) and LECs (CD31^{+}gp38^{+}) is shown. NS, not significant; $P > 0.05$. Data are representative of at least three independent experiments with at least three mice per group.

macrophages. Co-staining with the pan lymphatic marker, LYVE1, revealed substantial co-localization with eGFP, indicating that the lymphatic endothelium has the potential for *Il7* expression (Fig. 2A). Although it has been reported that a subset of tissue-resident macrophages is also LYVE1$^+$, co-staining was performed for CD11b (a pan-macrophage marker) (29). Although CD11b signal was spatially associated with the eGFP signal, careful examination of individual optical slices from the confocal stack revealed a complete absence of co-localization (Fig. 2B), suggesting that only LYVE1$^+$ LECs express *Il7* message in this region of the node.

To more specifically identify the phenotype of *Il7*-expressing cell types in LNs, we performed flow cytometry analysis on single-cell suspensions derived by enzymatic digestion of tissues from *Il7*$^{+/eGFP}$ mice. Stromal cells were pre-enriched by magnetic bead depletion of CD45$^+$ hematopoietic cells, after which four populations were readily identified by surface expression of gp38 (podoplanin, pan lymphatic marker) and CD31 (pan endothelial cell marker), as previously described (16). In agreement with the immunofluorescent tissue staining described, the brightest and most consistently observed population of eGFP$^+$ cells within the LNs displayed the characteristic surface phenotype of LECs, staining positively for both gp38 and CD31 (Fig. 2C) and *LYVE1* mRNA was restricted to this gp38$^+$CD31$^+$ population among flow-sorted cells (Fig. 2D). In addition to LECs, a dim signal for eGFP was detected within gp38$^+$CD31$^-$ FRCs, but not in the two other stromal cell populations (Fig. 2C and Supplementary Figure 1B, available at *International Immunology* Online). Consistent with the eGFP$^+$ signal observed by flow cytometry, *Il7* message was more readily detected by RT–PCR in sorted LECs and FRCs than in blood vessel endothelial cells (BECs) (Fig. 2D). These results show that the primary *Il7*-expressing stromal cells in resting LNs are LECs and FRCs.

eGFP expression was also evaluated within hematopoietic cell subpopulations in six separate gates defined on the basis of CD11c and CD11b surface phenotype, as previously described (29). Because the eGFP signal observed by immunofluorescence was closely associated with CD11b staining, we were particularly interested in CD11b$^+$ myeloid subsets. In agreement with the immunofluorescence analysis, no eGFP fluorescence was detected in any of the DC or macrophage populations, including plasmacytoid dendritic cells (pDCs) (Supplementary Figure 1C, available at *International Immunology* Online).

LECs throughout the body express IL-7

The prominent localization of eGFP to the subcapsular sinus and medullary region in *Il7*$^{+/eGFP}$ LNs raised the possibility that LECs throughout the body may be a significant source of IL-7 for re-circulating hematopoietic cells. To address this question, we examined other peripheral lymphatic beds for eGFP expression. *Il7*$^{eGFP/eGFP}$ mice were used for these histological experiments to maximize eGFP detection and eliminate any possible variable expression that could result from allelic exclusion (30). The central tendon of the diaphragm provides an ideal tissue for visualization of initial and draining lymphatics (31). Whole-mount staining and confocal microscopy of the central tendon of *Il7* $^{eGFP/eGFP}$ mice revealed an extensive network of eGFP$^+$ lymphatic vessels (Fig. 3A). Both morphological appearance and LYVE1 co-localization confirmed

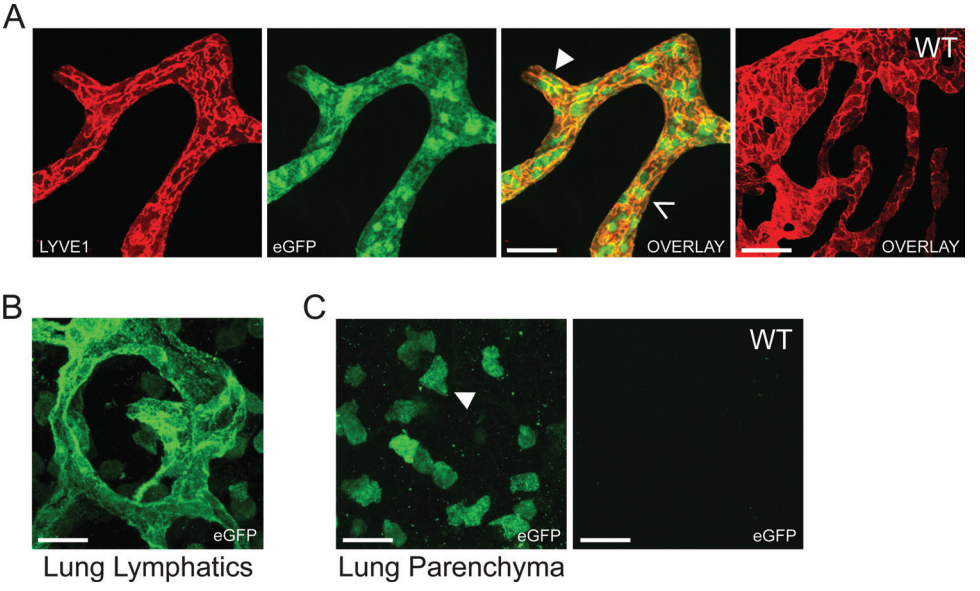

Fig. 3. Systemic lymphatics draining non-lymphoid tissues also express eGFP reporter protein. Immunofluorescence analysis to assess the expression of eGFP reporter protein in perfusion-fixed diaphragm and lung from *Il7*$^{eGFP/eGFP}$ mice. (A) Immunofluorescence microscopy for eGFP (green) and LYVE1 (red) in whole-mount central tendon of diaphragm. Filled arrow points to initial lymphatic and open arrow points to medium-sized collecting lymphatic. Left three panels are from *Il7*$^{eGFP/eGFP}$ mice and right panel is from WT control. Scale bar represents 50 μm. (B and C) Immunofluorescence microscopy for eGFP in 200-μm lung cryosections. Magnification ×100. Scale bars represent 20 μm. (B) Lymphatic vasculature of *Il7*$^{eGFP/eGFP}$. (C) Lung parenchyma of *Il7*$^{eGFP/eGFP}$ (left panel) and WT (right panel) control. Filled arrow points to a parenchymal cell. Data are representative of three experiments with three mice per group.

these structures to be lymphatic as opposed to blood vessel endothelium.

We next examined solid tissues with a prominent role in immune surveillance. The lung is a mucosal barrier at which there is constant exposure to airborne particulates, including potentially pathogenic micro-organisms. Its parenchyma includes a large population of hematopoietic cells, including γδ T cells, DCs and macrophages, as well as an extensive lymphatic drainage (32). Thick tissue sections from optimal cutting temperature compound-embedded lungs harvested from *Il7*$^{eGFP/eGFP}$ KO mice revealed cells with bright eGFP expression (Fig. 3B and C). In contrast to the pattern seen in the central tendon, the eGFP signal was not restricted to vascular structures but was also distributed throughout the lung parenchyma. The vascular eGFP signal was associated with lymphatic channels, following small and large airways before extending into the parenchyma of the tissue (Fig. 3B), whereas the remainder of the eGFP signal was associated with parenchymal cells of the lung (Fig. 3C).

To confirm the identity of the eGFP$^+$ cells in the lung, we enzymatically dissociated lung tissue from *Il7*$^{+/eGFP}$ mice and analyzed the resultant cell suspension by flow cytometry. Stromal populations (CD45$^+$ bead depleted) were delineated based on side scatter (SSC) and expression of CD31, EpCAM (pan epithelial marker) and gp38. Bulk endothelial cells were defined as SSC^{lo}CD31$^+$ and a presumptive LEC population within this group was identified by gp38 surface expression. Within the CD45$^-$SSC^{lo}CD31$^+$gp38$^+$EpCAM$^-$ cell subset was a well-defined population of eGFP^{bright} cells, in agreement with the immunofluorescence analysis (Fig. 4A and Supplementary Figure 2A, available at *International Immunology* Online). Flow sorting and RT–PCR analysis revealed that this population expresses high levels of mRNA for *eGFP*, *Il7* and the lymphatic-specific transcription factor, *Prox1*, definitively characterizing these cells as LECs (Fig. 4B) (33). Taken together with the observations that some LECs from LNs and the central tendon of the diaphragm also strongly express *Il7* message, this result suggests that most, if not all, tissues throughout the body contain LECs expressing *Il7* message. Interestingly, lung-derived LECs contained more *Il7* message than did LN LECs or LN FRCs (Fig. 4B).

The SSC^{hi}CD31$^-$ cell population in the lung has previously been shown to contain Type II alveolar epithelial cells (AECs), responsible for surfactant production and replacing damaged terminally differentiated Type I AECs (34, 35). Interestingly, these SSC^{hi} events contained a population of EpCAM$^+$ cells that were eGFP^{dim} (Fig. 4A and Supplementary Figure 2B, available at *International Immunology* Online). Upon sort purification, these Type II AECs showed detectable levels of *Il7* and high levels of surfactant protein B mRNA (Fig. 4B). Thus, resting Type II AECs express low levels of *Il7*. Interestingly, there was good agreement between *eGFP* and *Il7* transcript levels in LECs but not in Type II AECs. Given that Type II AECs are the vastly more abundant cell type, this latter pattern was reflected at the tissue level (Fig. 1E). As in the case of LNs, no eGFP was detected in any of the CD45$^+$ lung subsets examined, including both CD11c$^+$ DCs and CD11b$^+$ macrophages (data not shown).

Given the finding that LECs throughout the body actively produced *Il7* mRNA, we wished to know whether cells trafficking through the lymphatic compartment might be exposed to levels of IL-7 sufficient to result in signal transduction across the IL-7R. To address this possibility, we used intracellular 'Phosflow' to measure the level of phosphorylated STAT5 (pSTAT5) (downstream of IL-7R signaling) within CD3$^+$ T cells from blood, LNs or efferent lymphatic vessels (36, 37). CD3$^+$ T cells collected from both LNs and efferent lymphatics had higher pSTAT5 levels as compared with those from whole blood (Fig. 4C). The median fluorescence intensity of pSTAT5 in these compartments was approximately 2-fold that of the whole-blood cells (Fig. 4D). However, because pSTAT5 is not specific to the IL-7 pathway, we also examined IL-7R (CD127) surface levels on CD4$^+$ and CD8$^+$ T cells within the blood and efferent lymphatics (38). Previous studies have shown that IL-7 binding to the IL-7R causes rapid internalization and down-regulation of the receptor (39, 40). Both CD4$^+$ and CD8$^+$ T cells from efferent lymph had lower surface CD127 levels as compared with whole blood (Fig. 4E). Taken together, these data suggest that T cells moving through and exiting from LNs are exposed to higher levels of IL-7 than those circulating in blood.

Blockade of lymphocyte ingress into LNs induces up-regulation of Il7 expression in stromal cells

Given our hypothesis that lymphopenia results in up-regulation of IL-7 production, we might expect higher *Il7* expression levels in *Il7-eGFP* heterozygotes that display a mild congenital lymphopenia (Fig. 1D). Compared with WT mice, however, *Il7* mRNA expression levels in these mice were diminished (to about one-half) across a broad range of tissues, including LNs (Fig. 5A). Because, in the absence of a compensatory feedback mechanism, mRNA levels in these mono-allelic animals are expected to be at 50% of WT, *Il7* expression appears not to be regulated in mild congenital lymphopenia.

We next examined changes in *Il7* expression in response to severe depletion of T cells from the LNs, a situation more closely approximating the depletion seen in HIV infection (6). Using blocking monoclonal antibodies against α_4 and α_L integrins (required for lymphocyte ingress into the LNs), we were able to achieve a rapid and substantial depletion of T lymphocytes from the LNs *in vivo* (41). Treatment of *Il7*$^{+/eGFP}$ mice with the blocking antibodies for 22 days resulted in a 95% reduction in both CD4$^+$ and CD8$^+$ T cells found in LNs and a 50% increase of such cells in blood (Fig. 5B). The overall size of peripheral LNs (pLNs) from the antibody-treated mice was dramatically reduced compared with untreated controls (data not shown). Such a reduction in LN cellularity tends to bias whole-tissue RT–PCR data toward an increase in *Il7* mRNA because the T-cell subset contributes large numbers of housekeeping mRNA transcripts but not *Il7* transcripts. To avoid this possible confounder, we measured mRNA expression of flow-sorted CD45$^-$gp38$^+$ stromal cells, CD11c$^+$ DCs and CD11b$^+$ macrophages (Fig. 5C). After 22 days of antibody blockade, *Il7* mRNA levels were increased in the stromal subset by as much as 5-fold (Fig. 5D). Though *Il7* mRNA was also detected in CD11c$^+$ and CD11b$^+$ myeloid cells, the signal was 400-fold less than that detected in stromal cells. Animals treated with blocking antibodies for shorter intervals

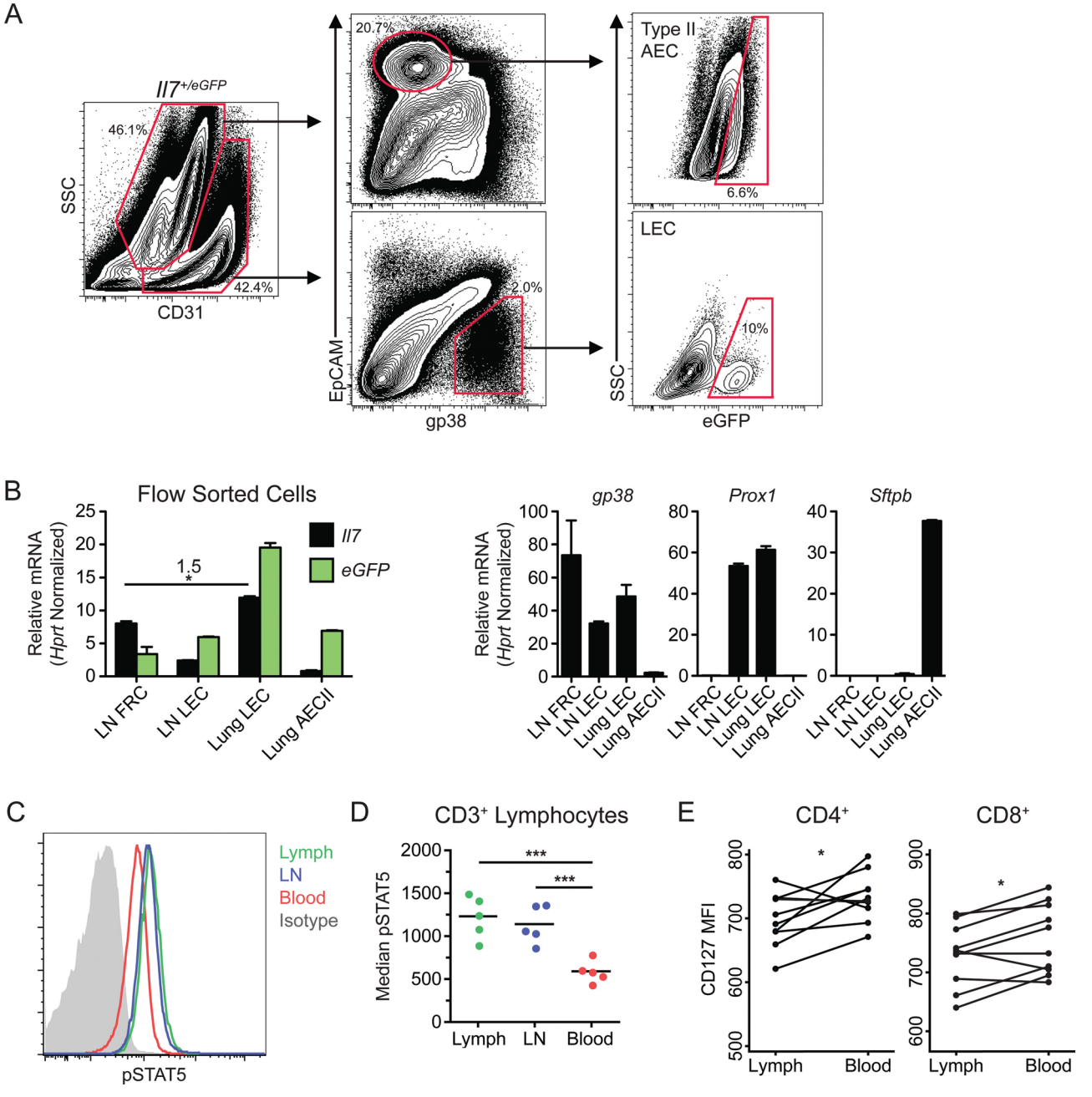

Fig. 4. LECs distributed throughout peripheral tissues express important amounts of IL-7. (A) Flow cytometry analysis of pooled single-cell suspensions prepared by enzymatic digestion of lungs from *Il7*$^{+/eGFP}$ heterozygote mice. Stromal cells enriched by CD45$^+$ cell depletion were stained for gp38, EpCAM and CD31 and analyzed. (B) Quantitative RT–PCR analysis of flow-sorted cells derived from lungs of *Il7-eGFP* heterozygotes. Stromal cells enriched by CD45$^+$ cell depletion were stained for CD45, gp38 and CD31 (LN) or gp38, EpCAM and CD31 (lung) and sorted by FACS into four populations: LN FRCs (gp38$^+$CD31$^-$), LN LECs (gp38$^+$CD31$^+$), lung Type II AECs (SSC^{hi}CD31$^-$gp38$^-$EpCAM$^+$; lung AECII) or lung LECs (SSC^{lo}CD31$^+$gp38$^+$ EpCAM$^-$). Purified RNA from each population was analyzed by quantitative RT–PCR. Data are from two groups of five mice and are representative of two separate experiments. *$P < 0.05$. (C and D) Flow analysis of pSTAT5 in T cells collected from whole blood, LNs or draining lymph of WT mice. Single-cell suspensions were stained for CD3 and intracellular pSTAT5. (C) Concatenated pSTAT5 histograms from five animals illustrating differences between compartments. (D) Median intracellular pSTAT5 fluorescence level (with isotype control subtracted) for each of the five animals in panel (C) is shown. ***$P < 0.001$. (E) Flow analysis of surface CD127 levels on T cells collected from whole blood or draining lymph. Cells were stained for CD3, CD4, CD8 and CD127 and median fluorescence intensity of CD127 was compared between compartments with a paired *t*-test. *$P < 0.05$.

also displayed a similar pattern of up-regulation of *Il7* expression (Fig. 5E). These observations indicate that *Il7* mRNA expression is increased when lymphocyte numbers decrease in the LNs and that CD45$^-$gp38$^+$ stromal cells represent the dominant population responding to acute lymphocyte depletion in the LNs.

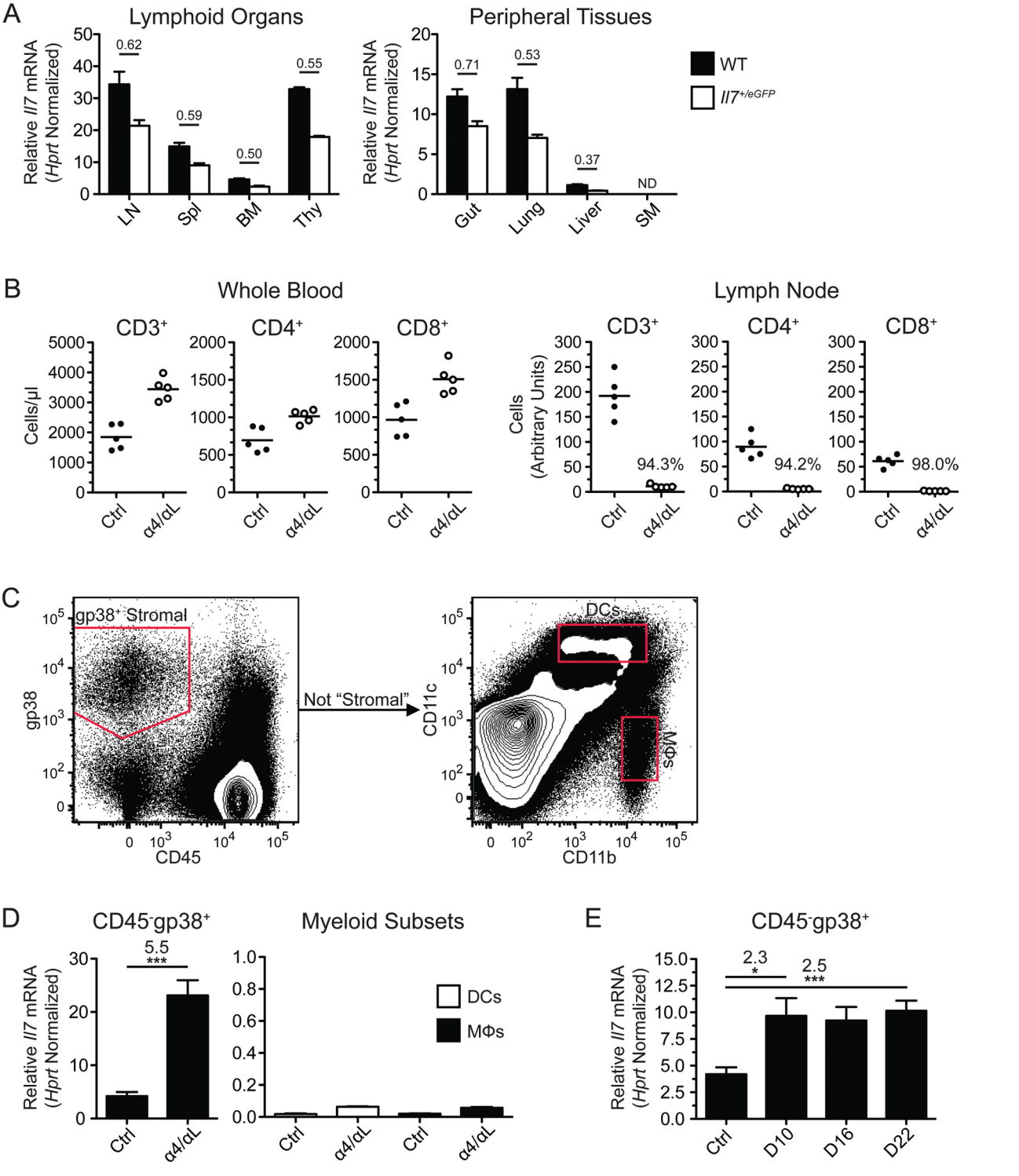

Fig. 5. Blockade of lymphocyte ingress into LNs induces stromal up-regulation of *Il7* mRNA. (A) Whole-tissue RT–PCR analysis of *Il7* transcript in tissues harvested from *Il7*$^{+/eGFP}$ mice. Signal was normalized to *Hprt*. Data are representative of two separate experiments with five mice in each group. The ratio of *Il7* transcript from WT to that from *Il7*$^{+/eGFP}$ heterozygotes is shown for inguinal lymph nodes (LN), spleen (Spl), BM, thymus (Thy), gut, lung, liver and skeletal muscle (SM). ND, not detected. (B) Absolute lymphocyte count in whole blood or enzymatically dispersed LNs of WT mice after treatment with either anti-α4/αL antibody (α4/αL) or isotype control antibody (Ctrl). Percent depletion is shown for LN subsets. (C–E) Analysis of single-cell suspensions from enzymatically dispersed LNs of WT mice stained for CD45, gp38, CD11b and CD11c. (C) Flow analysis and sorting gates. (D) Quantitative RT–PCR analysis of *Il7* transcript in sorted populations from LNs harvested from isotype control-treated (Ctrl) or α4/αL antibody (α4/αL) -treated (22 days) mice. CD45$^-$ stromal (CD45$^-$gp38$^+$) and myeloid (CD11c$^+$ DCs or CD11c$^-$CD11b$^+$ macrophages) cells were analyzed. Data are representative of at least two experiments with at least three mice per group. (E) Quantitative RT–PCR analysis of *Il7* transcript in flow-sorted CD45$^-$ stromal (CD45$^-$gp38$^+$) cells over time. Animals were treated for 10, 16 or 22 days with anti-α4/αL blocking antibodies (α4/αL) or isotype control antibody (Ctrl). $^*P < 0.05$, $^{***}P < 0.001$.

Hematopoietic cells are minor contributors to LN IL-7

Previous studies have suggested a myeloid contribution to IL-7 production, particularly in the setting of lymphocyte depletion (6, 42). To maximize our experimental sensitivity to *Il7* expression within myeloid cells, we generated BM chimeras in which only hematopoietic cells were capable of transcribing *Il7* (WT BM > *Il7*$^{eGFP/eGFP}$) or *eGFP* (*Il7*$^{eGFP/eGFP}$ BM > WT). In addition, because α_4 and α_L antibody blockade increased *Il7* transcript within pLNs, we reasoned that blockade might further promote detection of *Il7*- or *eGFP*-expressing hematopoietic cell types. As expected, chimeras on a WT stromal background effectively reconstituted their peripheral circulating lymphocyte pool, whereas chimeras on an *Il7* $^{eGFP/eGFP}$ background remained lymphopenic (Fig. 6A). Cell counting from dispersed LNs confirmed the efficacy of antibody blockade (Fig. 6B), and antibody staining and flow analysis of LNs and spleen confirmed the seeding of secondary lymphoid organs (SLOs) with myeloid cells originating from the transferred BM, including DCs, macrophages and pDCs (Fig. 6C).

RT–PCR analysis of whole LNs, including pLNs (e.g. inguinal, axillary and brachial LNs) and mesenteric LNs (mLNs), collected from *Il7*$^{eGFP/eGFP}$ BM > WT chimeras revealed that antibody blockade induced an increase in *Il7* mRNA, as for non-chimeric WT animals (Fig. 6D). Even under antibody blockade, however, *Il7*$^{eGFP/eGFP}$ BM > WT chimeras (expressing *Il7* message only in stromal cells) had 86.7-fold more *Il7* mRNA in mLNs and 22.3-fold more in spleen than did WT BM > *Il7*$^{eGFP/eGFP}$ chimeras (Fig. 6D), showing that stromal cells are the dominant source of IL-7 in lymphocyte-depleted nodes. However, these WT BM > *Il7*$^{eGFP/eGFP}$ chimeras contain a myeloid compartment that exists in an environment without stromal IL-7. To rule out the possibility that stromal IL-7 might be required for *Il7* transcription in myeloid cells, we stained tissue sections from *Il7*$^{eGFP/eGFP}$ BM > WT chimeras for eGFP (signifying *Il7* promoter activity in hematopoietic cells). We found that these animals had virtually undetectable eGFP signal, whereas WT BM > *Il7*$^{eGFP/eGFP}$ animals had robust eGFP expression (Fig. 6E). Thus, the myeloid compartment does not generate a significant amount of IL-7, even after lymphocyte depletion of the LNs.

Discussion

We developed an *Il7-eGFP* knock-in mouse that reports *Il7* transcription from the endogenous locus. Immunofluorescent and flow cytometric analyses revealed unexpectedly bright eGFP fluorescence within LYVE1$^+$gp38$^+$ LECs, both within the LN and non-SLO peripheral lymphatic beds (e.g. in the central tendon of the diaphragm and in the lung). Furthermore, LECs from targeted *Il7-eGFP* heterozygotes and WT littermates expressed *Il7* mRNA at a level comparable to that seen in LN FRCs, cells previously reported to produce IL-7 (16). Although LECs represent a relatively minor population within the LNs, their wide distribution throughout the body and their central role in immune cell trafficking suggest that they may contribute substantially to total body IL-7 production. Indeed, lymphocytes isolated from LNs or efferent lymph fluid had similar levels of pSTAT5 (and higher levels than those found within circulating lymphocytes in the blood), implying comparable exposure to IL-7. It has been suggested that access of lymphocytes to secondary lymphoid tissues, and particularly to the FRCs of the node parenchyma, is critical for naive T-cell homeostasis (16). Our data support the idea that circulating lymphocytes are likely exposed to IL-7 whenever they traffic through the extensive lymphatic network, which is constructed largely of LECs.

These experiments reveal a dynamic interplay between lymphocytes and the adherent structural and functional cells that define SLOs. Thus, acute blockade of lymphocyte entry into pLNs induced a rapid increase in *Il7* mRNA within CD45$^-$gp38$^+$ stromal cells. This group of cells contains FRCs that ensheath LN conduits within the T-cell zone as well as LECs that line the subcapsular sinus and the medullary cords. Although gp38 is a reliable marker for these two stromal elements, the CD45$^-$gp38$^+$ population is likely to be far more heterogeneous than is currently appreciated (43). For this reason, it is not possible to conclude with certainty whether the increase in stromal *Il7* described here represents an up-regulation of *Il7* via increased promoter activity or an increased frequency of an *Il7*-producing cell type within this broadly defined pool.

Recently, Kataru *et al.* (44) elegantly demonstrated that T cells (in contrast to B cells, macrophages and DCs) negatively regulate LN lymphatic vessel formation. Paracrine signaling via IFN-γ was found to inhibit LEC-specific gene expression and to reduce lymphatic vessel formation and, in this way, the T-cell mass within the node established the density of lymphatic vessels. Because LECs are a major source of IL-7 within the LNs and systemically, it is possible that increased lymphatic vessel formation in the absence of T cells underlies the increased *Il7* message observed in this study. We previously reported that the lymphocyte-depleted nodes of HIV-infected patients had an increased frequency and signal intensity of cells staining for IL-7 and that many of these cells expressed myeloid cell markers (6); in this study, however, we were unable to detect a significant myeloid cell-derived *Il7* signal. Because the lymphatic vasculature of the node is closely associated with a rich network of interdigitating macrophages (29), the discovery that LECs make a significant contribution to LN IL-7 production could provide an explanation for our previous findings.

Our finding that the systemic lymphatics express IL-7 suggests that cells other than T cells might be influenced by the cytokine. Although it has been shown that a small subset of naive T cells re-circulate through peripheral tissues, the afferent lymphatic system is generally associated with trafficking of activated antigen-presenting cells (APCs). Migratory DCs express both IL-7Rα and γc and therefore possess the necessary cell-surface receptors to bind IL-7 (45, 46). Recent evidence suggests that IL-7 is capable of enhancing the potency of an adaptive immune response. Pellegrini *et al.* (47) showed that systemic IL-7 treatment during a chronic infection of mice with lymphocytic choriomeningitis virus (LCMV) promoted immunity by boosting effector T-cell function and numbers and amplifying cytokine production. Although these effects may be mediated via direct signaling to T cells, as the authors suggest, IL-7 effects on APCs could also contribute to enhanced T-cell activation and cytokine production. Additional co-stimulation induced by IL-7 might shape the nature of the response, in a similar manner to thymic stromal lymphopoietin (TSLP). Indeed, the initial report describing the T_h-polarizing effects of

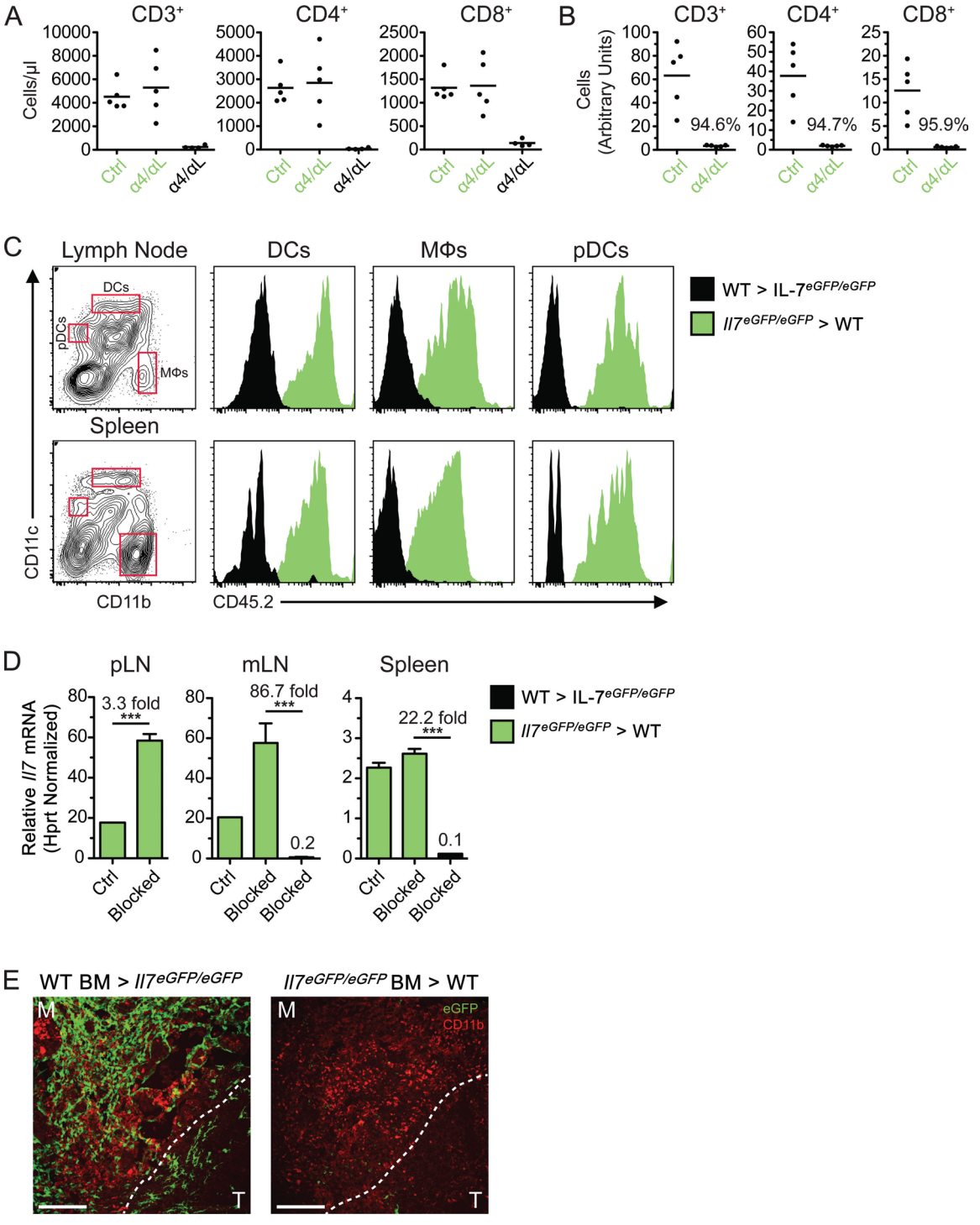

Fig. 6. Hematopoietic cells make a minor contribution to LN IL-7. (A–D) Bone marrow chimeras of WT BM > *Il7*$^{eGFP/eGFP}$ recipients (n = 4, black) or *Il7*$^{eGFP/eGFP}$ BM > WT recipients (n = 10, green). Cells derived from WT mice were CD45.1$^+$, whereas those from *Il7*$^{eGFP/eGFP}$ mice were CD45.2$^+$. (A and B) Absolute lymphocyte counts in whole blood (A) and LNs (B) measured by staining with antibodies for CD3, CD4 and CD8. Percent depletion is shown in (B) over antibody-blocked (α4/αL) animals. Ctrl, non-antibody depleted; α4/αL, antibody-blocked. (C) Efficient seeding of SLOs with myeloid cells originating from transferred BM. Enzymatically dispersed mLNs or splenic cell suspensions were stained with CD11c, CD11b and CD45.2 and plotted. The black histogram shows reconstitution in a single representative WT BM > *Il7*$^{eGFP/eGFP}$ chimera and the green histogram is representative of reconstitution in a single *Il7*$^{eGFP/eGFP}$ BM > WT chimera. (D) Quantitative RT–PCR analysis of whole-tissue RNA collected from pLNs, mLNs or spleen of chimeric animals without (Ctrl) and with antibody blockade (blocked) for 22 days. Fold difference in *Il7* transcript is shown in some cases. ***$P < 0.001$. (E) Immunofluorescence analysis of perfusion-fixed 20-µm cryosections from mLNs harvested from chimeric animals following antibody blockade (22 days): eGFP (green) and CD11b (red). Data are representative of at least four animals. M, medullary region; T, T cell area. Scale bar represents 100 µm.

TSLP on DCs also demonstrated that IL-7 had similar polarizing effects on DCs (45).

Four groups have described *Il7* reporter models in which a bacterial artificial chromosome (BAC) transgenic approach was utilized (27, 48–50). Although all the reporter mice had activity in the thymus, only two had detectable activity in other tissues known to express endogenous *Il7* transcript (9, 10, 13–20). Despite this variability in expression, these reporters have provided significant insights into IL-7 biology and are the subject of an excellent review (51). Recently, Onder *et al.* (22) further characterized reporter expression from their BAC *Il7-eYFP* mice. Similar to our findings, they describe significant eYFP signal within the LEC subset. Interestingly, LN LEC eYFP was induced by LCMV infection and eYFP$^+$ LN LECs were also important for LN reconstruction. One potential concern with BAC reporters is the separation of reporter expression from nearby endogenous regulatory regions and local chromatin remodeling events, potentially influencing reporter fidelity. By contrast, the *Il7-eGFP* knock-in mouse described in this study faithfully reports *Il7* transcription from the endogenous locus in a broad range of tissues, similar to that just reported by Hara *et al.* (21). Notably, their knock-in mice were also found to have significant eGFP within LN LECs as well as thymus, spleen, BM and gut. Treatment of these animals with dextran sodium sulfate led to significant induction of gut eGFP. Taken together with our data, these recent studies provide indisputable evidence that both LNs and systemic LECs are a potent source of IL-7 and provide important examples of *in vivo* peripheral IL-7 regulation.

The reporter construct used in the generation of our *Il7-eGFP* knock-in mice includes an SV40 early polyadenylation signal after the *eGFP* stop codon. Inclusion of this sequence not only stabilizes reporter transcripts but also removes potential downstream regulatory elements, particularly those located within the 3′ UTR. Such elements are known to play an important role in post-transcriptional regulation of other cytokines (52, 53). In addition, to enhance the *eGFP* signal, we deleted a portion of the 5′ UTR (191 of 247 base pairs) that has been previously shown to suppress translation (54). During our characterization of the *Il7-eGFP* reporter, we noted marked differences in the *Il7:eGFP* transcript ratios in certain tissues. Tissue-specific (e.g. LN versus lung) and cell-type-specific (e.g. lung LECs versus AECs) differences in this ratio might be related to post-transcriptional regulation that cannot operate on the targeted allele. This possibility warrants further investigation and the *Il7-eGFP* reporter may be an important resource in this work.

In sum, we show that multiple cell types across many different tissues express substantial levels of *Il7* mRNA and that LECs are an important source of *in vivo* IL-7, as recently described elsewhere (21, 22). This result raises the following question: which sites are the most important for T-cell homeostasis? This issue will be difficult to address until a conditional and tissue-specific *Il7*$^{-/-}$ mouse is generated. Such a tool will be invaluable to our understanding of how specific compartments contribute to the overall homeostasis of the immune system.

Supplementary data

Supplementary data are available at *International Immunology* Online.

Funding

National Institutes of Health (DPI OD00329, R37 AI40312 and U01AI43864 to J.M.M. and 5K23AI081540 to D.J.H.-O.); Harvey V. Berneking Living Trust; National Institutes of Health Medical Scientist Training Program (GM007618 to C.N.M.). J.M.M. is a recipient of the National Institutes of Health Director's Pioneer Award Program, part of the National Institutes of Health Roadmap for Medical Research (DPI OD00329).

Acknowledgements

We thank T. Ho and B. Hyun for help with flow sorting, N. Killeen and the UCSF Mouse Genetics Core for injecting ES cell clones with the targeted *Il7-eGFP* allele and generating the chimeras and M. Premenko-Lanier for help with generation of BM chimeras. We also thank E. Sharpe and M. J. Broadhurst for expert technical assistance.

Author contributions

C.N.M. and D.J.H.-O. designed, conducted and analyzed the experiments and wrote the manuscript; M.S.L. designed and made the *Il7-eGFP* mouse and wrote the manuscript; G.L. did immunofluorescence analysis and confocal microscopy; I.P.C. and M.M. did lymph collection; D.M.M. supervised immunofluorescence experiments; S.R.C. supervised the lymph experiments and J.M.M. supervised research and wrote the manuscript.

Conflict of interest statement: The authors declare no competing financial interests.

References

1 Carrette, F. and Surh, C. D. 2012. IL-7 signaling and CD127 receptor regulation in the control of T cell homeostasis. *Semin. Immunol.* 24:209.
2 Ceredig, R. and Rolink, A. G. 2012. The key role of IL-7 in lymphopoiesis. *Semin. Immunol.* 24:159.
3 Peschon, J. J., Morrissey, P. J., Grabstein, K. H. *et al.* 1994. Early lymphocyte expansion is severely impaired in interleukin 7 receptor-deficient mice. *J. Exp. Med.* 180:1955.
4 Puel, A., Ziegler, S. F., Buckley, R. H. and Leonard, W. J. 1998. Defective IL-7R expression in T(-)B(+)NK(+) severe combined immunodeficiency. *Nat. Genet.* 20:394.
5 von Freeden-Jeffry, U., Vieira, P., Lucian, L. A., McNeil, T., Burdach, S. E. and Murray, R. 1995. Lymphopenia in interleukin (IL)-7 gene-deleted mice identifies IL-7 as a nonredundant cytokine. *J. Exp. Med.* 181:1519.
6 Napolitano, L. A., Grant, R. M., Deeks, S. G. *et al.* 2001. Increased production of IL-7 accompanies HIV-1-mediated T-cell depletion: implications for T-cell homeostasis. *Nat. Med.* 7:73
7 Bolotin, E., Annett, G., Parkman, R. and Weinberg, K. 1999. Serum levels of IL-7 in bone marrow transplant recipients: relationship to clinical characteristics and lymphocyte count. *Bone Marrow Transplant.* 23:783.
8 Fry, T. J., Connick, E., Falloon, J. *et al.* 2001. A potential role for interleukin-7 in T-cell homeostasis. *Blood* 97:2983.
9 Funk, P. E., Stephan, R. P. and Witte, P. L. 1995. Vascular cell adhesion molecule 1-positive reticular cells express interleukin-7 and stem cell factor in the bone marrow. *Blood* 86:2661.
10 Tokoyoda, K., Egawa, T., Sugiyama, T., Choi, B. I. and Nagasawa, T. 2004. Cellular niches controlling B lymphocyte behavior within bone marrow during development. *Immunity* 20:707.
11 Wu, J. Y., Purton, L. E., Rodda, S. J. *et al.* 2008. Osteoblastic regulation of B lymphopoiesis is mediated by Gs{alpha}-dependent signaling pathways. *Proc. Natl. Acad. Sci. U.S.A.* 105:16976.

12 Faas, S. J., Rothstein, J. L., Kreider, B. L., Rovera, G. and Knowles, B. B. 1993. Phenotypically diverse mouse thymic stromal cell lines which induce proliferation and differentiation of hematopoietic cells. *Eur. J. Immunol.* 23:1201.
13 Zamisch, M., Moore-Scott, B., Su, D. M., Lucas, P. J., Manley, N. and Richie, E. R. 2005. Ontogeny and regulation of IL-7-expressing thymic epithelial cells. *J. Immunol.* 174:60.
14 Zubkova, I., Mostowski, H. and Zaitseva, M. 2005. Up-regulation of IL-7, stromal-derived factor-1 alpha, thymus-expressed chemokine, and secondary lymphoid tissue chemokine gene expression in the stromal cells in response to thymocyte depletion: implication for thymus reconstitution. *J. Immunol.* 175:2321.
15 Heufler, C., Topar, G., Grasseger, A. *et al.* 1993. Interleukin 7 is produced by murine and human keratinocytes. *J. Exp. Med.* 178:1109.
16 Link, A., Vogt, T. K., Favre, S. *et al.* 2007. Fibroblastic reticular cells in lymph nodes regulate the homeostasis of naive T cells. *Nat. Immunol.* 8:1255.
17 Murray, A. M., Simm, B. and Beagley, K. W. 1998. Cytokine gene expression in murine fetal intestine: potential for extrathymic T cell development. *Cytokine* 10:337.
18 Rane, L., Rahman, S., Magalhaes, I. *et al.* 2011. Increased (6 exon) interleukin-7 production after M. tuberculosis infection and soluble interleukin-7 receptor expression in lung tissue. *Genes Immun.* 12:513.
19 Sawa, Y., Arima, Y., Ogura, H. *et al.* 2009. Hepatic interleukin-7 expression regulates T cell responses. *Immunity* 30:447.
20 Watanabe, M., Ueno, Y., Yajima, T. *et al.* 1995. Interleukin 7 is produced by human intestinal epithelial cells and regulates the proliferation of intestinal mucosal lymphocytes. *J. Clin. Invest.* 95:2945.
21 Hara, T., Shitara, S., Imai, K. *et al.* 2012. Identification of IL-7-producing cells in primary and secondary lymphoid organs using IL-7-GFP knock-in mice. *J. Immunol.* 189:1577.
22 Onder, L., Narang, P., Scandella, E. *et al.* 2012. IL-7-producing stromal cells are critical for lymph node remodeling. *Blood* 120:4675.
23 Mazzucchelli, R. and Durum, S. K. 2007. Interleukin-7 receptor expression: intelligent design. *Nat. Rev. Immunol.* 7:144.
24 Tang, J., Nuccie, B. L., Ritterman, I., Liesveld, J. L., Abboud, C. N. and Ryan, D. H. 1997. TGF-beta down-regulates stromal IL-7 secretion and inhibits proliferation of human B cell precursors. *J. Immunol.* 159:117.
25 Roye, O., Delhem, N., Trottein, F. *et al.* 1998. Dermal endothelial cells and keratinocytes produce IL-7 in vivo after human *Schistosoma mansoni* percutaneous infection. *J. Immunol.* 161:4161.
26 Churchman, S. M. and Ponchel, F. 2008. Interleukin-7 in rheumatoid arthritis. *Rheumatology (Oxford)* 47:753.
27 Shalapour, S., Deiser, K., Sercan, O. *et al.* 2010. Commensal microflora and interferon-gamma promote steady-state interleukin-7 production in vivo. *Eur. J. Immunol.* 40:2391.
28 Baluk, P., Tammela, T., Ator, E. *et al.* 2005. Pathogenesis of persistent lymphatic vessel hyperplasia in chronic airway inflammation. *J. Clin. Invest.* 115:247.
29 Phan, T. G., Green, J. A., Gray, E. E., Xu, Y. and Cyster, J. G. 2009. Immune complex relay by subcapsular sinus macrophages and noncognate B cells drives antibody affinity maturation. *Nat. Immunol.* 10:786.
30 Bix, M. and Locksley, R. M. 1998. Independent and epigenetic regulation of the interleukin-4 alleles in CD4+ T cells. *Science* 281:1352.
31 Shinohara, H. 1997. Lymphatic system of the mouse diaphragm: morphology and function of the lymphatic sieve. *Anat. Rec.* 249:6.
32 Holt, P. G., Strickland, D. H., Wikström, M. E. and Jahnsen, F. L. 2008. Regulation of immunological homeostasis in the respiratory tract. *Nat. Rev. Immunol.* 8:142.
33 Wigle, J. T., Harvey, N., Detmar, M. *et al.* 2002. An essential role for Prox1 in the induction of the lymphatic endothelial cell phenotype. *EMBO J.* 21:1505.
34 Mason, R. J. 2006. Biology of alveolar type II cells. *Respirology* 11(Suppl.):S12.
35 Gereke, M., Gröbe, L., Prettin, S. *et al.* 2007. Phenotypic alterations in type II alveolar epithelial cells in CD4+ T cell mediated lung inflammation. *Respir. Res.* 8:47.
36 Schweneker, M., Favre, D., Martin, J. N., Deeks, S. G. and McCune, J. M. 2008. HIV-induced changes in T cell signaling pathways. *J. Immunol.* 180:6490.
37 Foxwell, B. M., Beadling, C., Guschin, D., Kerr, I. and Cantrell, D. 1995. Interleukin-7 can induce the activation of Jak 1, Jak 3 and STAT 5 proteins in murine T cells. *Eur. J. Immunol.* 25:3041.
38 Wei, L., Laurence, A. and O'Shea, J. J. 2008. New insights into the roles of Stat5a/b and Stat3 in T cell development and differentiation. *Semin. Cell Dev. Biol.* 19:394.
39 Park, J. H., Yu, Q., Erman, B. *et al.* 2004. Suppression of IL-7Ralpha transcription by IL-7 and other prosurvival cytokines: a novel mechanism for maximizing IL-7-dependent T cell survival. *Immunity* 21:289.
40 Henriques, C. M., Rino, J., Nibbs, R. J., Graham, G. J. and Barata, J. T. 2010. IL-7 induces rapid clathrin-mediated internalization and JAK3-dependent degradation of IL-7Ralpha in T cells. *Blood* 115:3269.
41 Denucci, C. C., Mitchell, J. S. and Shimizu, Y. 2009. Integrin function in T-cell homing to lymphoid and nonlymphoid sites: getting there and staying there. *Crit. Rev. Immunol.* 29:87.
42 Guimond, M., Veenstra, R. G., Grindler, D. J. *et al.* 2009. Interleukin 7 signaling in dendritic cells regulates the homeostatic proliferation and niche size of CD4+ T cells. *Nat. Immunol.* 10:149.
43 Kang, J., Yoo, J., Lee, S., Tang, W., Aguilar, B., Ramu, S., Choi, I., Otu, H. H., Shin, J. W., Dotto, G. P., Koh, C. J., Detmar, M. and Hong, Y. K. 2010. An exquisite cross-control mechanism among endothelial cell fate regulators directs the plasticity and heterogeneity of lymphatic endothelial cells. *Blood* 116:140.
44 Kataru, R. P., Kim, H., Jang, C. *et al.* 2011. T lymphocytes negatively regulate lymph node lymphatic vessel formation. *Immunity* 34:96.
45 Soumelis, V., Reche, P. A., Kanzler, H. *et al.* 2002. Human epithelial cells trigger dendritic cell mediated allergic inflammation by producing TSLP. *Nat. Immunol.* 3:673.
46 Vogt, T. K., Link, A., Perrin, J., Finke, D. and Luther, S. A. 2009. Novel function for interleukin-7 in dendritic cell development. *Blood* 113:3961.
47 Pellegrini, M., Calzascia, T., Toe, J. G. *et al.* 2011. IL-7 engages multiple mechanisms to overcome chronic viral infection and limit organ pathology. *Cell* 144:601.
48 Mazzucchelli, R. I., Warming, S., Lawrence, S. M. *et al.* 2009. Visualization and identification of IL-7 producing cells in reporter mice. *PLoS ONE* 4:e7637.
49 Repass, J. F., Laurent, M. N., Carter, C. *et al.* 2009. IL-7-hCD25 and IL-7-Cre BAC transgenic mouse lines: new tools for analysis of IL-7 expressing cells. *Genesis* 47:281.
50 Alves, N. L., Richard-Le Goff, O., Huntington, N. D. *et al.* 2009. Characterization of the thymic IL-7 niche in vivo. *Proc. Natl. Acad. Sci. U.S.A.* 106:1512.
51 Kim, G. Y., Hong, C. and Park, J. H. 2011. Seeing is believing: illuminating the source of in vivo interleukin-7. *Immune Netw.* 11:1.
52 Powell, M. J., Thompson, S. A., Tone, Y., Waldmann, H. and Tone, M. 2000. Posttranscriptional regulation of IL-10 gene expression through sequences in the 3'-untranslated region. *J. Immunol.* 165:292.
53 Stoecklin, G., Lu, M., Rattenbacher, B. and Moroni, C. 2003. A constitutive decay element promotes tumor necrosis factor alpha mRNA degradation via an AU-rich element-independent pathway. *Mol. Cell. Biol.* 23:3506.
54 Namen, A. E., Lupton, S., Hjerrild, K. *et al.* 1988. Stimulation of B-cell progenitors by cloned murine interleukin-7. *Nature* 333: 571.